Electronic Supplementary Material (ESI) for Journal of Materials Chemistry C.

Side-chain Modification of Non-fullerene Acceptors for Organic Solar Cells with Efficiency over 18%

ZhiXiang Li‡[a], Changzun Jiang‡[a], Xin Chen[a], Guangkun Song[a], Xiangjian Wan[a], Bin Kan[c*], Tainan Duan[ad], Ekaterina A. Knyazeva[b], Oleg Alekseevich Rakitin[b] and Yongsheng Chen[a*]

[a]The Centre of Nanoscale Science and Technology and Key Laboratory of Functional Polymer Materials, Institute of Polymer Chemistry, State Key Laboratory of Elemento-Organic Chemistry, College of Chemistry, Haihe Laboratory of Sustainable Chemical Transformations, Renewable Energy Conversion and Storage Center (RECAST), Nankai University, 300071, Tianjin, China.

[b]N. D. Zelinsky Institute of Organic Chemistry Russian Academy of Sciences, 47 Leninsky Prospekt,119991, Moscow, Russia.

[c]School of Materials Science and Engineering, National Institute for Advanced Materials, Nankai University, 300350, Tianjin, China.

[d]Chongqing Institute of Green and Intelligent Technology, Chongqing School, University of Chinese Academy of Sciences (UCAS Chongqing), Chinese Academy of Sciences, 400417, Chongqing, China.

‡ These authors contributed equally to this work.

[*] Corresponding E-mails: yschen99@nankai.edu.cn (Y.C.); kanbin04@nankai.edu.cn (B. K.)

Content

1. Measurements and Instruments

The ^{1}H, ^{13}C nuclear magnetic resonance (NMR) spectra were taken on a Bruker AV400 Spectrometer. Matrix-assisted laser desorption/ionization time-of-flight (MALDI-TOF) mass spectrometry was performed on a Bruker Autoflex III instrument. Fourier transform mass spectrometry (FTMS) with high-resolution matrix-assisted laser desorption/ionization (HR-MALDI) was performed on a Varian 7.0T FTMS instrument. Ultraviolet-visible (UV-Vis) absorption spectra were measured on a UV-Vis instrument Agilent Cary 5000 UV-Vis-NIR spectrophotometer.

Cyclic voltammetry (CV) experiments were employed to evaluate the energy levels with an LK98B II Microcomputer-based Electrochemical Analyzer in acetonitrile solution at room temperature. The experiments were carried out in a conventional three-electrode configuration with a glassy carbon electrode as the working electrode, a saturated calomel electrode (SCE) as the reference electrode and a Pt wire as the counter electrode. Tetrabutylammonium phosphorus hexafluoride (Bu_4NPF_6, 0.1 M) in dry acetonitrile solution was used as the supporting electrolyte with the scan rate of 100 mV/s under the protection of nitrogen. The highest occupied molecular orbital (HOMO) and lowest unoccupied molecular orbital (LUMO) energy levels were calculated from the onset oxidation potential and the onset reduction potential, using the equation $E_{HOMO} = -(4.80+E_{ox}^{onset})$, $E_{LUMO} = -(4.80+E_{red}^{onset})$.

The current density-voltage (*J-V*) curves of photovoltaic devices were recorded by a Keithley 2400 source-measure unit. The photocurrent was measured under the simulated illumination of 100 mW cm^{-2} with AM 1.5 G using a Enli SS-F5-3A solar simulator, which was calibrated by a standard Si solar cell (made by Enli Technology Co., Ltd., Taiwan, and calibrated report can be traced to NREL). The thickness of the active layers was measured by a Veeco Dektak 150 profilometer. The EQE spectra were measured by using a QE-R Solar Cell Spectral Response Measurement System (Enli Technology Co., Ltd., Taiwan). EQE_{EL} measurements were performed by applying external voltage/current sources through the devices (REPS, Enlitech). The FTPS-EQE measurement was carried out on an Enlitech FTPS PECT-600 instrument. The operation stability tests were carried out on a commercial test system (PAS-GV, Enli Technology Co., Ltd., Taiwan). Continuous illumination was provided by an array of LED at 25 ± 2 °C. The performance evolution of devices was tracked under max power point in a glovebox filled with ultrahigh purity nitrogen (<0.1 ppm O_2 and H_2O) without encapsulation.

Atomic force microscope (AFM) investigation was performed using Bruker MultiMode 8 in tapping mode. The GIWAXS data were obtained at 1W1A Diffuse X-ray Scattering Station, Beijing Synchrotron Radiation Facility (BSRF-1W1A). The grazing incident angle was 0.2 degree, and the exposure time was 60 seconds.

The hole and electron mobility were measured using the space charge limited current (SCLC) method, employing a diode configuration of ITO/PEDOT:PSS/active layer/M_OO_3/Ag for holes and ITO/ZnO/PFN-Br/active layer/PDNIT-F3N/Ag for electrons by taking the dark current density and fitting the results to a space charge limited form, where SCLC is described by:

$$J = \frac{9\varepsilon_0 \varepsilon_r \mu V^2}{8L^3}$$

where J is the current density, L is the film thickness of the active layer, μ is the hole or electron mobility, ε_r is the relative dielectric constant of the transport medium, ε_0 is the permittivity of free space (8.85×10^{-12} F m^{-1}), V ($=V_{appl} - V_{bi}$) is the internal voltage in the device, where V_{appl} is the applied voltage to the device and V_{bi} is the built-in voltage due to the relative work function difference of the two electrodes.

2. Materials Synthesis and Characterization

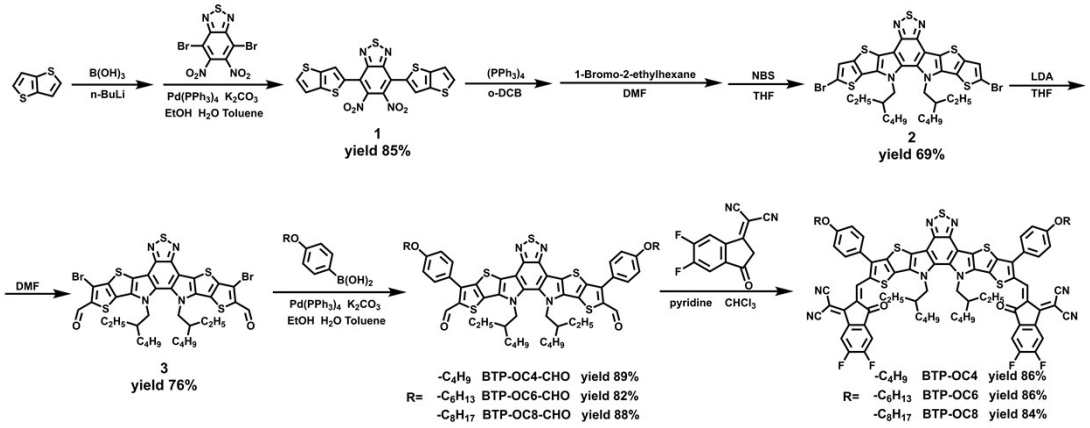

Figure S1. Synthetic route of acceptors.

Synthesis of compound 1

Thieno[3,2-b]thiophene (2.0 g, 14.3 mmol) was mixed with tetrahydrofuran (50 mL) and stirred at -78 ℃ under nitrogen, n-butyllithium (9.4 mL, 1.6 M in n-Hexane) was added slowly to the mixture. After stirring at -78 ℃ for 1 h, then trimethyl borate (3.12 g, 30.0 mmol) was added slowly to the mixture, the mixture was allowed to warm to room temperature and poured into water. The aqueous phase was extracted with ethyl acetate for three times. The organic phase was dried over sodium sulphate and concentrated under reduced pressure. The residue was then mixed with 4,7-Dibromo-5,6-dinitro-2,1,3-benzothiadiazole (2.30 g, 6.0 mmol), potassium carbonate (4.25 g, 30.8 mmol), tetrakis(triphenylphosphine)palladium (1.15 g, 1.0 mmol), toluene (50 mL), ethanol (10 mL) and water (10 mL), and stirred at 100 ℃ under nitrogen. After stirring for 10 h, the mixture was allowed to cool and poured into methanol. Then, through filter under reduced pressure to obtain the filter cake, then the filter cake washed with water, methanol and hexane. The residue red solid (2.56 g, 85%) was directly used for next step without further purification.

Synthesis of compound 2

Compound 1 (2.26 g, 5.1 mmol) was mixed with o-Dichlorobenzene (30 mL) and PPh_3 (5.00 g, 19.1 mmol), then stirred at 200 ℃ under argon. After stirring for 10 h, the mixture was allowed to cool and poured into methanol (100 mL). Then the mixture was filtered under reduced pressure and washed with hexane to obtain the filter cake. The resulted solid was then mixed with N,N-Dimethylformamide (30 mL) and potassium carbonate (4.15 g, 30.0 mmol) under argon, then the mixture was heated to 90 ℃. After stirring for 18 h, the mixture was allowed to cool and poured into water, the aqueous phase was extracted with dichloromethane for three times. The organic phase was dried over sodium sulphate and concentrated under

reduced pressure. The residue was recrystallized with chloroform and methanol and yellow solid was obtained. Then, N-bromosuccinimide (1.96 g, 11.0 mmol) and tetrahydrofuran (30 mL) was added to the yellow solid. After stirring at room temperature for 12 h, the mixture was poured into water. The aqueous phase was extracted with dichloromethane for three times. The organic phase was dried over sodium sulfate and concentrated under reduced pressure. The residue was purified with column chromatography over silica gel to yield **2** as red solid (2.86 g, 69%).

^{1}H NMR (400 MHz, Chloroform-*d*) δ 7.42 (s, 2H), 4.74 - 4.44 (m, 4H), 1.97 (h, *J* = 6.7, 6.2 Hz, 2H), 1.08 - 0.86 (m, 16H), 0.62 (m, 12H).

^{13}C NMR (101 MHz, Chloroform-*d*) δ 147.52, 139.77, 136.63, 131.65, 124.37, 124.13, 122.78, 111.63, 110.87, 54.96, 40.09, 29.63, 27.64, 23.12, 22.72, 13.71, 10.11.

Synthesis of compound 3

Compound 2 (1.64 g, 2.0 mmol) was mixed with tetrahydrofuran (30 mL) and stirred at -60 ℃ under nitrogen, lithium diisopropylamide (4.0 mL, 2 M in THF, 8.0 mmol) was added slowly to the mixture. After stirring at -60 ℃ for 1 h, the mixture was allowed to warm to stir at room temperature for 6h. Then, the mixture was cooled to -20 ℃, a mixed solvent of DMF:THF=1:3 (totally 12 mL) was added slowly to the mixture. The mixture was slowly warmed to room temperature, and poured into water. The aqueous phase was extracted with ethyl acetate for three times. The organic phase was dried over sodium sulfate and concentrated under reduced pressure. The residue was purified with column chromatography over silica gel to yield compound **3** as red solid (1.33 g, 76%).

^{1}H NMR (400 MHz, Chloroform-*d*) δ 10.15 (s, 2H), 4.63 (tt, *J* = 9.0, 4.2 Hz, 4H), 2.00 (hept, *J* = 6.5 Hz, 2H), 0.99 - 0.86 (m, 16H), 0.65 (m, 12H).

^{13}C NMR (101 MHz, Chloroform-*d*) δ 181.40, 147.25, 136.51, 133.97, 132.86, 132.84, 129.06, 128.74, 112.76, 55.35, 40.27, 29.60, 27.65, 23.08, 22.71, 13.70, 10.03.

Synthesis of compound BTP-OC4-CHO

Compound 3 (0.20 g, 0.23 mmol) was mixed with (4-Butoxyphenyl)boronic acid (0.19 g, 1.0 mmol), potassium carbonate (0.28 g, 2.0 mmol), tetrakis(triphenylphosphine)palladium (0.011 g, 0.010 mmol), toluene (30 mL), ethanol (5 mL) and water (5 mL), and stirred at 100 ℃ under nitrogen. After stirring for 10 h, the mixture was allowed to cool down and poured into water. The aqueous phase was extracted with dichloromethane for three times. The organic phase was dried over sodium sulfate and concentrated under reduced pressure. The residue was purified with column chromatography over silica gel. The obtained product was then recrystallized with

chloroform and methanol to yield **BTP-OC4-CHO** as yellow solid (0.21 g, 89%).

^{1}H NMR (400 MHz, Chloroform-*d*) δ 9.96 (d, *J* = 1.8 Hz, 2H), 7.71 (dd, *J* = 8.6, 1.9 Hz, 4H), 7.18-7.04 (m, 4H), 4.68 (t, *J* = 6.6 Hz, 4H), 4.09 (td, *J* = 6.5, 1.8 Hz, 4H), 2.05 (d, *J* = 10.0 Hz, 2H), 1.85 (dt, *J* = 12.7, 6.2 Hz, 4H), 1.62 - 1.51 (m, 6H), 1.15 - 0.91 (m, 20H), 0.75 - 0.54 (m, 12H).

^{13}C NMR (101 MHz, Chloroform-*d*) δ 184.16, 160.55, 147.55, 145.57, 142.95, 136.88, 136.71, 132.76, 132.73, 131.02, 129.12, 127.80, 124.07, 115.31, 112.48, 68.01, 55.24, 40.23, 31.27, 29.63, 27.62, 23.08, 22.73, 19.28, 13.88, 13.70, 10.05.

Synthesis of compound BTP-OC6-CHO

Compound **BTP-OC6-CHO** was prepared following the same procedure as for **BTP-OC4-CHO**. The product was afforded as a yellow solid (0.20 g, 82%).

^{1}H NMR (600 MHz, Chloroform-*d*) δ 8.83 (s, 2H), 8.50 (t, *J* = 8.1 Hz, 2H), 7.72 (t, *J* = 7.4 Hz, 2H), 7.62 (d, *J* = 8.2 Hz, 4H), 7.16 (d, *J* = 8.2 Hz, 4H), 4.79 (p, *J* = 15.7, 15.2 Hz, 4H), 4.11 (t, *J* = 6.7 Hz, 4H), 2.13 (p, *J* = 6.9, 6.5 Hz, 2H), 1.88 (p, *J* = 6.9 Hz, 4H), 1.58 - 1.48 (m, 4H), 1.40 (d, *J* = 6.8 Hz, 8H), 1.24 - 0.91 (m, 22H), 0.73 (m, 12H).

^{13}C NMR (101 MHz, Chloroform-*d*) δ 184.10, 160.53, 147.49, 145.50, 142.89, 136.87, 136.69, 132.72, 132.69, 131.01, 129.11, 127.72, 127.70, 124.05, 115.29, 112.46, 68.31, 55.26, 40.24, 31.62, 29.64, 29.20, 27.65, 25.77, 23.11, 23.09, 22.77, 22.66, 14.09, 13.74, 10.08.

Synthesis of compound BTP-OC8-CHO

Compound **BTP-OC8-CHO** was prepared following the same procedure as for **BTP-OC4-CHO**. The product was afforded as a yellow solid (0.23 g, 88%).

^{1}H NMR (400 MHz, Chloroform-*d*) δ 9.95 (s, 2H), 7.68 (d, *J* = 8.6 Hz, 4H), 7.08 (d, *J* = 8.7 Hz, 4H), 4.72 (h, *J* = 7.3, 6.8 Hz, 4H), 4.05 (t, *J* = 6.5 Hz, 4H), 2.08 (p, *J* = 6.9 Hz, 2H), 1.85 (q, *J* = 7.5, 7.1 Hz, 4H), 1.50 (t, *J* = 7.7 Hz, 4H), 1.37 - 0.88 (m, 38H), 0.76 - 0.57 (m, 12H).

^{13}C NMR (101 MHz, Chloroform-*d*) δ 184.05, 160.52, 147.46, 145.45, 142.87, 136.85, 136.68, 132.69, 132.66, 130.99, 129.08, 127.68, 127.66, 124.04, 115.28, 112.45, 68.29, 40.24, 31.85, 29.66, 29.39, 29.28, 29.23, 27.65, 26.09, 23.11, 22.76, 22.70, 19.06, 14.14, 13.72, 10.08.

Synthesis of compound BTP-OC4

BTP-OC4-CHO (0.10 g, 0.10 mmol) was mixed with 2-(5,6-dichloro-3-oxo-2,3-dihydro-1H-inden-1-ylidene)malononitrile (100 mg, 0.38 mmol), pyridine (0.5 mL) and chloroform (30 mL). The mixture was stirred at reflux for 12 h under nitrogen. After cooling down to room temperature, the mixture was poured into methanol (150 mL) and filtered. The residue was

purified by column chromatography on silica gel using petroleum ether/dichloromethane (2:1) as eluent yielding a purple solid (0.12 g, 86 %).

^{1}H NMR (400 MHz, Chloroform-*d*) δ 8.82 (s, 2H), 8.49 (dd, *J* = 9.9, 6.4 Hz, 2H), 7.72 (t, *J* = 7.4 Hz, 2H), 7.62 (d, *J* = 8.2 Hz, 4H), 7.16 (d, *J* = 8.3 Hz, 4H), 4.79 (d, *J* = 8.1 Hz, 4H), 4.12 (t, *J* = 6.5 Hz, 4H), 2.23-2.04 (m, 2H), 1.94 - 1.80 (m, 4H), 1.56 (dd, *J* = 9.8, 5.2 Hz, 4H), 1.25 - 0.97 (m, 22H), 0.80 - 0.61 (m, 12H).

^{13}C NMR (101 MHz, Chloroform-*d*) δ 185.81, 161.29, 158.83, 153.13, 153.01, 152.88, 151.88, 147.47, 144.63, 138.90, 137.67, 136.69, 136.61, 134.86, 134.40, 133.69, 133.03, 131.78, 131.24, 124.46, 120.92, 115.88, 114.85, 114.64, 113.68, 113.56, 112.60, 112.40, 77.22, 69.19, 68.11, 55.63, 40.44, 31.22, 29.72, 27.72, 23.18, 22.85, 19.27, 13.91, 13.78, 10.19.

Synthesis of compound BTP-OC6

Compound **BTP-OC6** was prepared following the same procedure as for **BTP-OC4**. The product was afforded as a purple solid (0.13g, 86%).

^{1}H NMR (600 MHz, Chloroform-*d*) δ 8.83 (s, 2H), 8.50 (t, *J* = 8.0 Hz, 2H), 7.72 (t, *J* = 7.4 Hz, 2H), 7.62 (d, *J* = 8.2 Hz, 4H), 7.16 (d, *J* = 8.2 Hz, 4H), 4.80 (dt, *J* = 19.4, 9.2 Hz, 4H), 4.11 (t, *J* = 6.7 Hz, 4H), 2.13 (p, *J* = 7.0, 6.6 Hz, 2H), 1.88 (p, *J* = 6.9 Hz, 4H), 1.69 - 1.42 (m, 4H), 1.40 (d, *J* = 6.8 Hz, 6H), 1.22 (tt, *J* = 14.7, 6.6 Hz, 4H), 1.15 - 0.95 (m, 24H), 0.73 (m, 8H).

^{13}C NMR (151 MHz, Chloroform-*d*) δ 185.81, 161.29, 158.86, 155.17, 151.89, 147.50, 144.64, 138.91, 137.68, 136.69, 134.86, 134.45, 133.72, 133.02, 131.77, 131.27, 124.46, 120.94, 115.87, 114.82, 114.63, 113.68, 113.56, 112.57, 112.44, 69.21, 68.43, 55.63, 40.43, 31.62, 29.71, 29.14, 27.71, 25.72, 23.17, 22.84, 22.64, 14.08, 13.77, 10.07.

Synthesis of compound BTP-OC8

Compound **BTP-OC8** was prepared following the same procedure as for **BTP-OC4**. The product was afforded as a purple solid (0.12 g, 84%).

^{1}H NMR (600 MHz, Chloroform-*d*) δ 8.83 (s, 2H), 8.50 (dd, *J* = 9.7, 6.2 Hz, 2H), 7.72 (t, *J* = 7.4 Hz, 2H), 7.62 (d, *J* = 8.2 Hz, 4H), 7.16 (d, *J* = 8.2 Hz, 4H), 5.04-4.57 (m, 4H), 4.11 (t, *J* = 6.6 Hz, 4H), 2.12 (p, *J* = 6.8 Hz, 2H), 1.88 (p, *J* = 6.8 Hz, 4H), 1.52 (d, *J* = 7.9 Hz, 4H), 1.42 - 0.88 (m, 38H), 0.72 (m, 12H).

^{13}C NMR (151 MHz, Chloroform-*d*) δ 185.83, 161.31, 158.87, 153.47, 151.91, 147.51, 144.65, 138.93, 137.69, 136.70, 134.87, 134.43, 133.73, 133.03, 131.79, 131.28, 124.47, 120.95, 115.88, 114.84, 114.64, 113.70, 113.57, 112.46, 69.22, 68.45, 55.64, 40.44, 31.86, 29.72, 29.42, 29.29, 29.20, 27.73, 26.07, 23.19, 22.85, 22.71, 14.16, 13.79, 10.09.

3. Device Fabrication

The OSCs were fabricated with a conventional structure of ITO/PEDOT:PSS/Active layer/PDINO/Ag. First, ITO-coated glass was cleaned with deionized water, acetone, and isopropyl alcohol under ultrasonication for sequentially 15 mins. Second, the surface of ITO-coated glass was treated in an ultraviolet-ozone chamber for 15 min. A thin layer of PEDOT: PSS (Baytron P VP AI 4083) was deposited on the ITO substrate at 4300 rpm for 20 s and then dried at 150 ℃ for 20 mins in air. Then the substrates were transferred to a glovebox filled with nitrogen. The PM6: BTP-OCs (1:1.2 *w*/*w*) was dissolved in chloroform at the total blend concentration of 13.2 mg/mL with 0.5vt% 1-Chloronaphthalene (1-CN) as the additive. The active layer was spun onto the PEDOT: PSS layer at 2000 rpm for 30 s, and then the films were treated with thermal annealing at 100 ℃ for 5 min. After cooled down, the methanol solution of PDINO (2 mg/mL) was spin-coated on the top of the active layer at 3000 rpm for 20 s. Finally, Ag electrode with the thickness of 150 nm was evaporated under 2×10^{-6} Pa. The active area of device was 4 mm^2 and the thickness is 105 nm.

4. The Calculation Method of E_{loss}

E_{loss} can be calculated by the equation:

$$E_{loss} = E_g - qV_{oc}$$

Where E_g can be calculated by the crossing point of normalized absorption and photoluminescence spectra.

The detailed components of E_{loss} can be categorized into three parts based on the Shockley-Queisser (SQ) limit[2-4]:

$$E_{loss} = (E_g - qV_{oc}^{SQ}) + (qV_{oc}^{SQ} - qV_{oc}^{rad}) + (qV_{oc}^{rad} - qV_{oc})$$

Where

$$V_{oc}^{SQ} = \frac{kT}{q}\ln\left(\frac{J_{sc}^{SQ}}{J_0^{SQ}} + 1\right) \cong \frac{kT}{q}\ln\left(\frac{q \cdot \int_{E_g}^{+\infty} \emptyset_{AM1.5G}(E)dE}{q \cdot \int_{E_g}^{+\infty} \emptyset_{BB}(E)dE}\right)$$

Where $\emptyset_{BB}(E)$ is black body emission at room temperature. Thus, for the unavoidable radiative recombination ΔE_1:

$$\Delta E_1 = E_g - qV_{oc}^{SQ}$$

$$V_{oc}^{rad} = \frac{kT}{q}\ln\left(\frac{J_{sc}}{J_0^{rad}} + 1\right) \cong \frac{kT}{q}\ln\left(\frac{q \cdot \int_0^{+\infty} EQE(E)\emptyset_{AM1.5G}(E)dE}{q \cdot \int_0^{+\infty} EQE(E)\emptyset_{BB}(E)dE}\right)$$

Thus, for the radiative recombination ΔE_2

$$\Delta E_2 = qV_{oc}^{SQ} - qV_{oc}^{rad}$$

Finally, for the non-radiative recombination loss ΔE_3

$$\Delta E_3 = qV_{oc}^{rad} - qV_{oc}$$

Where V_{OC} is the open circuit voltage of the OSC.

5. Figures and Tables

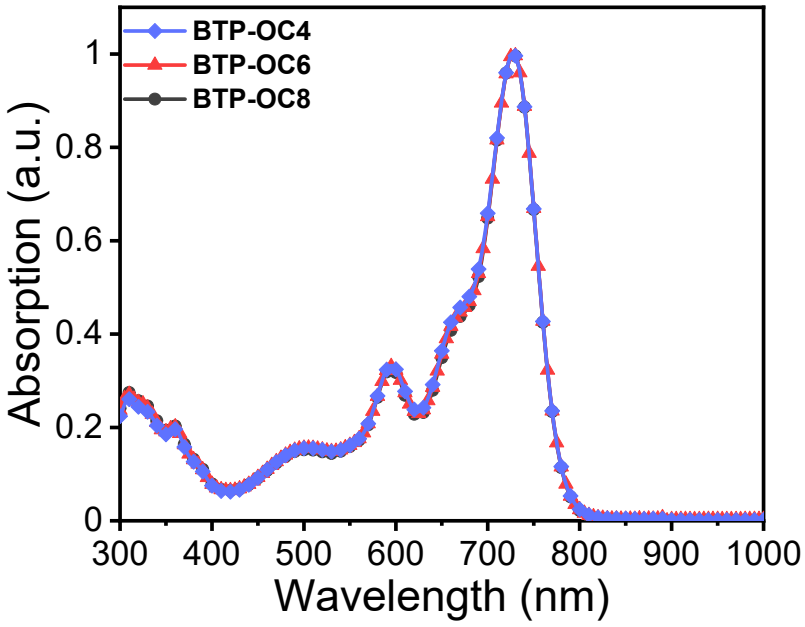

Figure S2. Normalized UV-vis absorption spectra of acceptors in CF solution.

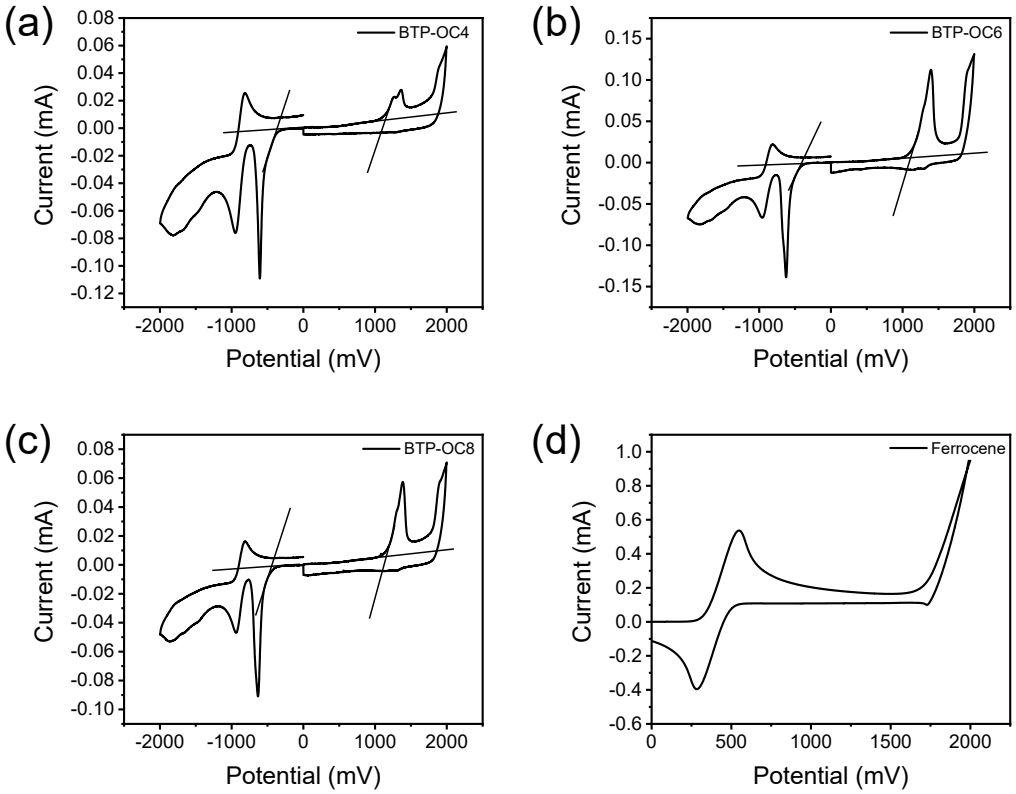

Figure S3. Cyclic voltammetry plots of BTP-OC4/6/8 films and Ferrocene, respectively.

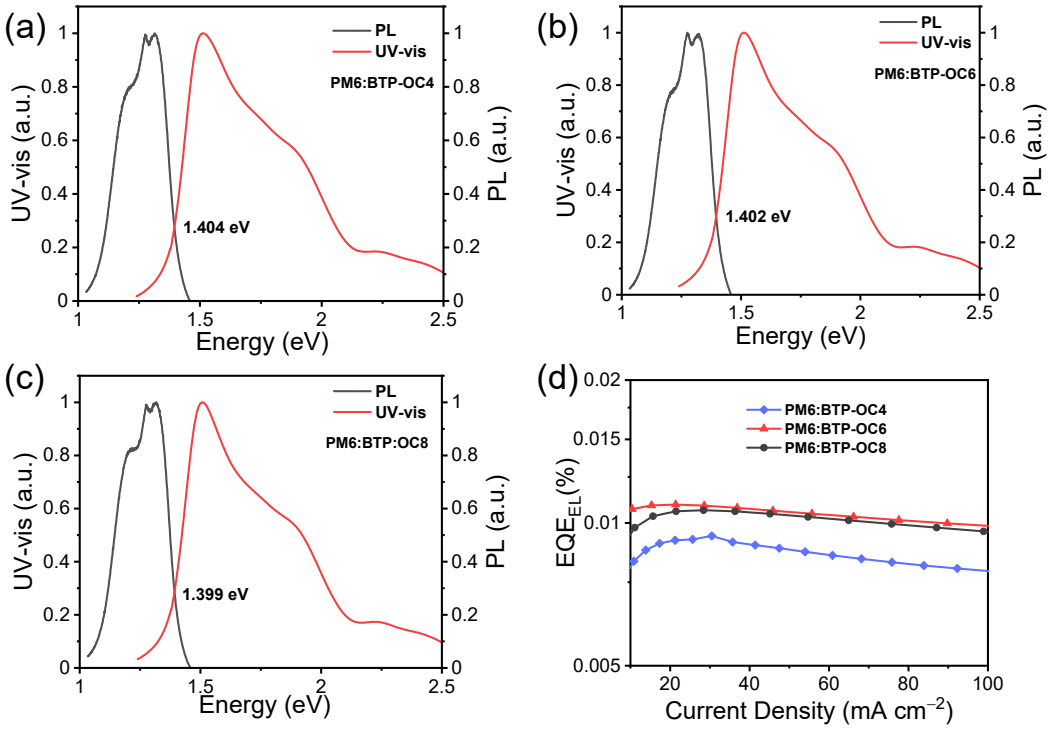

Figure S4. (a-c) Normalized absorption and PL spectra of BTP-OC series films, (d) EL quantum efficiencies under different injected current densities.

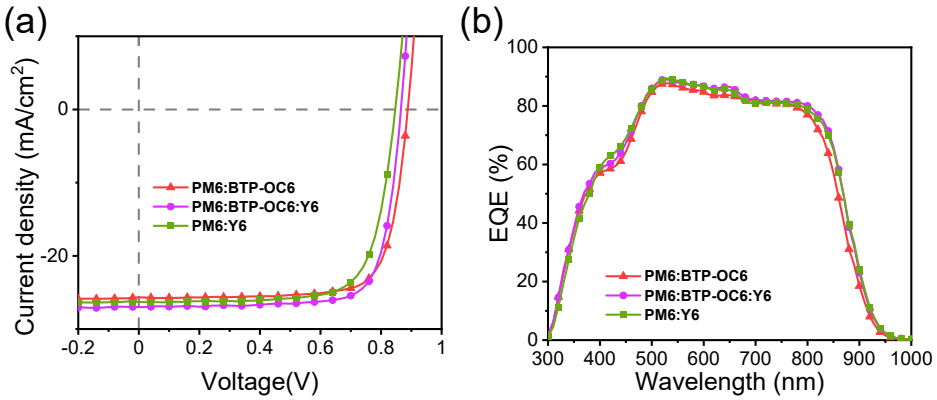

Figure S5. (a) *J-V* curves under simulated AM 1.5 G illumination, and (b) Corresponding EQE spectra of the devices based on PM6:BTP-OC6 binary system and PM6:BTP-OC6:Y6 ternary system.

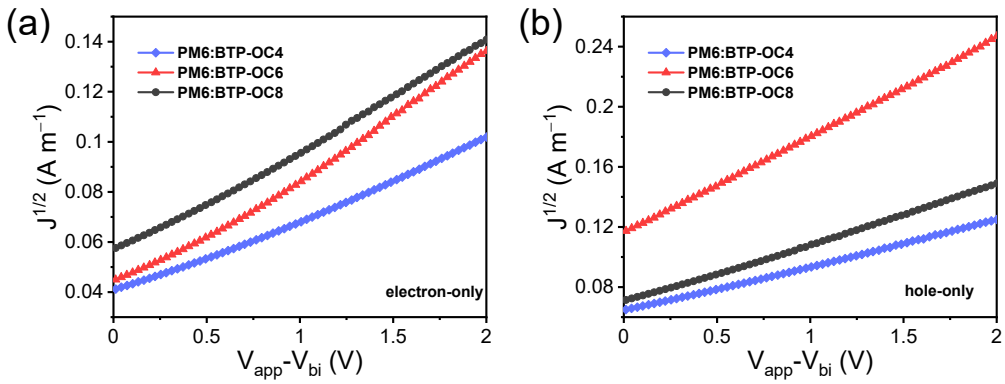

Figure S6. the $J^{1/2}$–V plots for the (a) electron-only and (b) hole-only of devices based on BTP-OC4, BTP-OC6 and BTP-OC8, respectively.

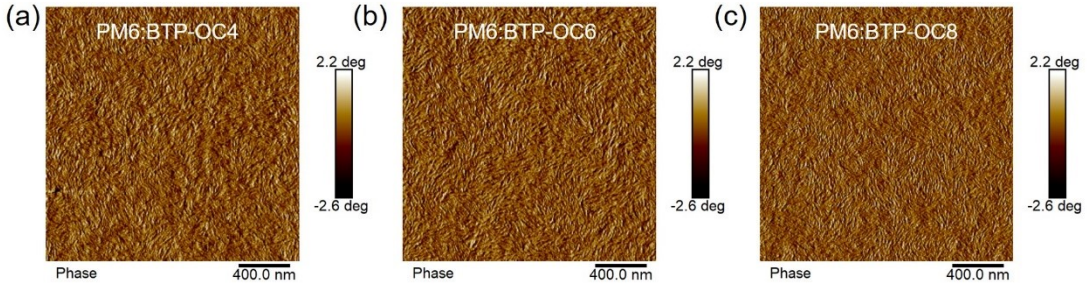

Figure S7. AFM phase images of the three blend films.

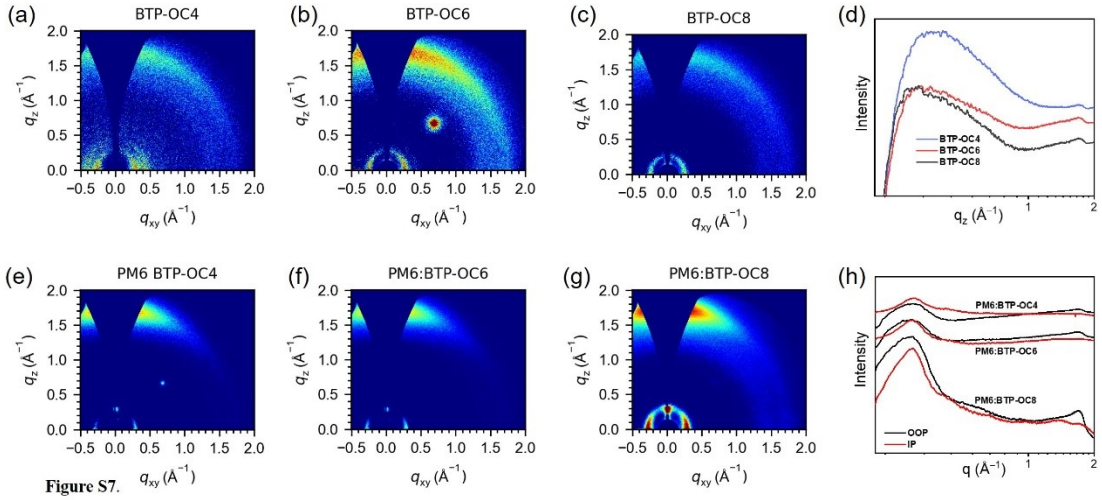

Figure S8. (a-c) 2D-GIWAXS patterns for pure BTP-OC4, BTP-OC6 and BTP-OC8 films. (d) Out-of-plane line cuts of the GIWAXS patterns for the pure films. (e-g) 2D-GIWAXS patterns for PM6:BTP-OC4, PM6:BTP-OC6 and PM6:BTP-OC8 blend films. (h) In-plane and out-of-plane line cuts of GIWAXS patterns for the blend films.

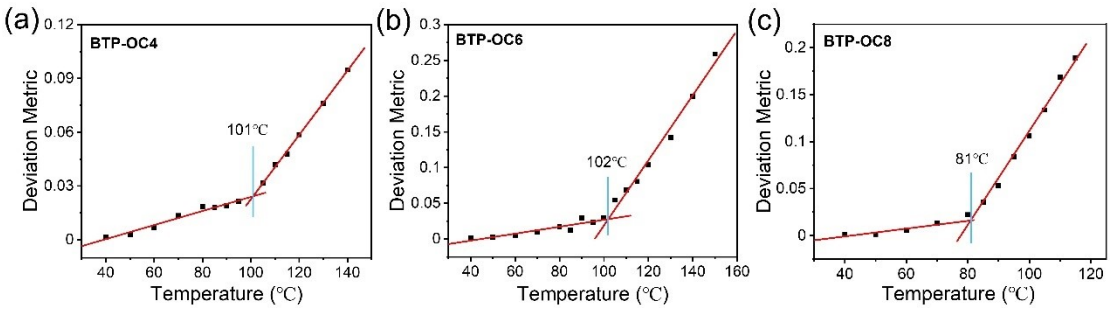

Figure S9. UV-vis deviation metric results of (a) BTP-OC4, (b) BTP-OC6 and (c) BTP-OC8.

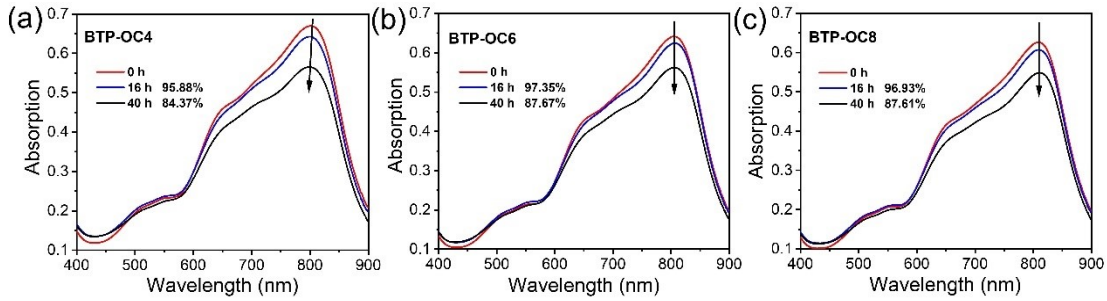

Figure S10. The UV-vis absorption spectra of (a) BTP-OC4, (b) BTP-OC6 and (c) BTP-OC8 on neat film state with different exposing time under continuous UV illumination (365 nm, 40 mW cm^{-2}) in ambient condition.

Table S1. Photovoltaic performance of solar cells based on PM6:BTP-OC6 (1:1.2, w/w) blend films with different additive contents.

CN (vt%)	V_{OC} (V)	J_{SC}(mA/cm^2)	FF (%)	PCE (%)
0.3	0.882	24.84	74.78	16.38
0.5	0.889	25.66	77.14	17.59
0.7	0.878	24.11	75.81	16.04

Table S2. Photovoltaic performance of solar cells based on PM6:BTP-OC6 (0.5 vt% CN) blend films with different thermal annealing (TA) temperature.

TA (°C)	V_{OC} (V)	J_{SC}(mA/cm^2)	FF (%)	PCE (%)
80	0.890	24.03	76.42	16.35
100	0.889	25.66	77.14	17.59
120	0.883	25.06	74.33	16.46

Table S3. Performance of the OSCs with different PM6 (D)/BTP-OC6 (A) ratios (0.5 vt% CN, 100 °C TA).

D:A	V_{OC} (V)	J_{SC}(mA/cm^2)	FF (%)	PCE (%)
1:1	0.889	25.56	75.84	17.23
1:1.2	0.889	25.66	77.14	17.59
1:1.4	0.880	25.76	74.98	17.00

Table S4. Detailed Energy Loss of Optimal OSCs Based on PM6:BTP-OC4, PM6:BTP-OC6 and BTP-OC8.

Acceptor	[a]E_g (eV)	V_{oc} (V)	[b]$V_{oc,sq}$ (V)	[c]$V_{oc,rad}$ (V)	ΔE_1 (eV)	ΔE_2 (eV)	[1]ΔE_3 (eV)	[2]ΔE_3 (eV)	E_{loss} (eV)
BTP-OC4	1.404	0.885	1.142	1.089	0.262	0.053	0.204	0.242	0.519
BTP-OC6	1.402	0.889	1.140	1.078	0.262	0.062	0.189	0.236	0.513
BTP-OC8	1.399	0.882	1.138	1.072	0.261	0.066	0.190	0.237	0.517

[a] E_g was estimated via the crossing points between normalized absorption and PL spectra of neat FOM series films. [b] $V_{oc,sq}$ is calculated according to the SQ limit. [c] $V_{oc,rad}$ is the V_{oc} when there is only radiative recombination and are calculated from EQE, FTPS-EQE and EL measurements. $\Delta E_1 = E_g - V_{oc,sq}$. ΔE_3 ($\Delta E_3 = q\Delta V_{nr}$) is determined by two approaches: 1) calculated by $q(V_{oc,rad} - V_{oc})$ and 2) obtained from the equation $q\Delta V_{nr} = -kT\ln EQE_{EL}$ by measuring the device EQE_{EL}.

Table S5. The hole mobility and electron mobility for the hole-only and electron-only devices based on BTP-OC4, BTP-OC6 and BTP-OC8.

Blend Film	μ_h (10^{-4} cm^2 V^{-1} s^{-1})	μ_e (10^{-4} cm^2 V^{-1} s^{-1})	μ_h/μ_e
PM6:BTP-OC4	3.35	2.40	1.40
PM6:BTP-OC6	6.35	5.74	1.11
PM6:BTP-OC8	4.61	3.50	1.32

Table S6. Summary of the GIWAXS parameters for the neat acceptor films and blend films.

Film	(010)				(100)	
	q (Å^{-1})	d[a] (Å)	FWHM (Å^{-1})	CCL[b] (Å)	q (Å^{-1})	d[a] (Å)
BTP-OC4	1.688	3.722	0.210	26.960	0.253	24.835
BTP-OC6	1.690	3.718	0.207	27.333	0.250	25.133
BTP-OC8	1.690	3.718	0.209	27.015	0.248	25.335
PM6:BTP-OC4	1.688	3.722	0.283	19.998	0.303	20.737
PM6:BTP-OC6	1.688	3.722	0.223	25.317	0.298	21.085
PM6:BTP-OC8	1.675	3.751	0.240	23.519	0.298	21.085

[a]Calculated from the equation: d-spacing = 2π/q. [b]Obtained from the Scherrer equation: CCL = 2 πK/FWHM, where FWHM is the full-width at half-maximum and K is a shape factor (K = 0.9).

Table S7. Differences of three acceptors and their OSCs.

Acceptors	Side Chain	T_g (°C)	PCE (%)	Thermal stability[a]	Photo-stability[b]
BTP-OC4	butoxy	101	16.45	71.0%	86.6%
BTP-OC6	hexyloxy	102	17.59	74.6%	94.4%
BTP-OC8	octyloxy	81	16.88	68.2%	93.1%

[a] PCE maintained after continues heated for 350 h under 65 °C in glovebox.
[b] PCE maintained under MPP tracking for 120 h in glovebox.

Table S8. Photovoltaic parameters of OSCs based on Y6 derivatives through side-chain engineering.

No.	Active layer	V_{OC} [V]	J_{SC} [mA cm^{-2}]	FF [%]	PCE [%]	Refs.
1	PM6: BTP-4F-P2EH	0.880	25.85	80.08	18.22	1
2	PM6:N3	0.837	25.81	73.9	15.98	2
3	PTQ10:m-BTP-C6Ph	0.883	25.3	79.3	17.7	3
4	PBQ6:m-TEH	0.880	26.61	79.03	18.51	4
5	PM6: BTP-PhC6	0.865	25.0	77.0	16.7	5
6	PM6:BTP-eC9	0.839	26.2	81.1	17.8	6
7	PM6:Y6-O	0.95	22.4	78.0	16.6	7
8	PM6: EH-HD-4F	0.84	27.5	79.3	18.38	8
9	PM6:L8-BO	0.87	25.72	81.5	18.32	9
	This work	0.889	25.66	77.14	17.59	

6. NMR figures

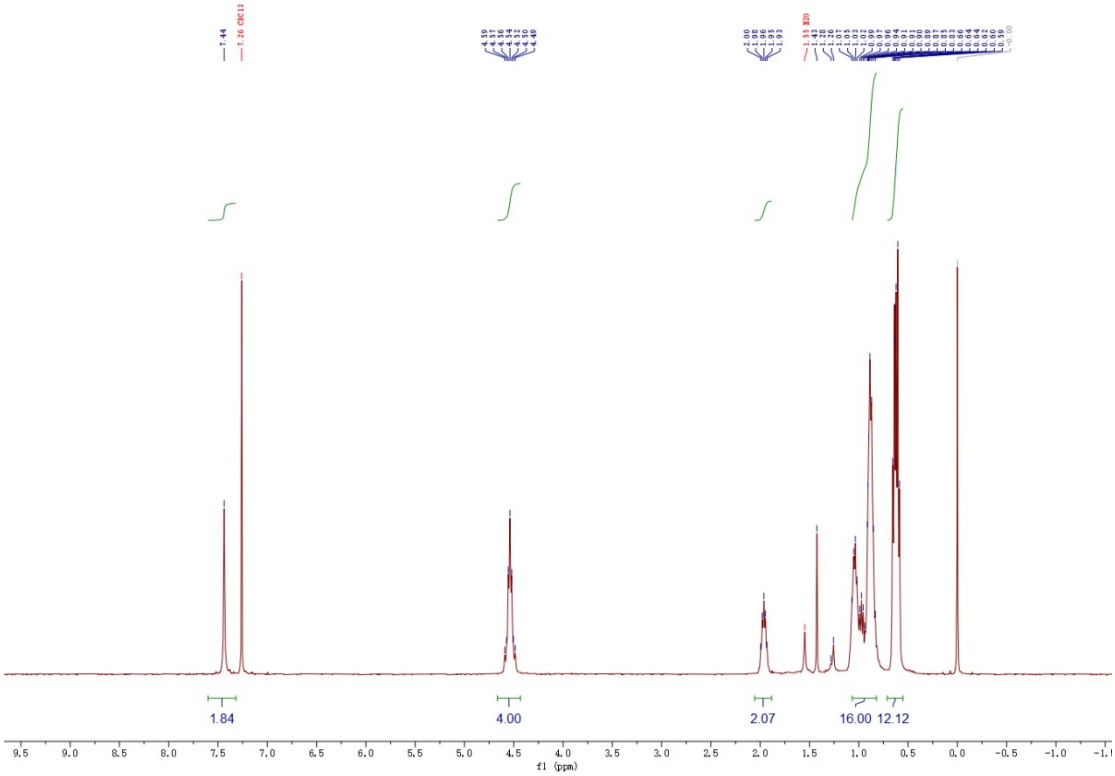

Figure S11. ^{1}H NMR (400 MHz) of **compound 2**.

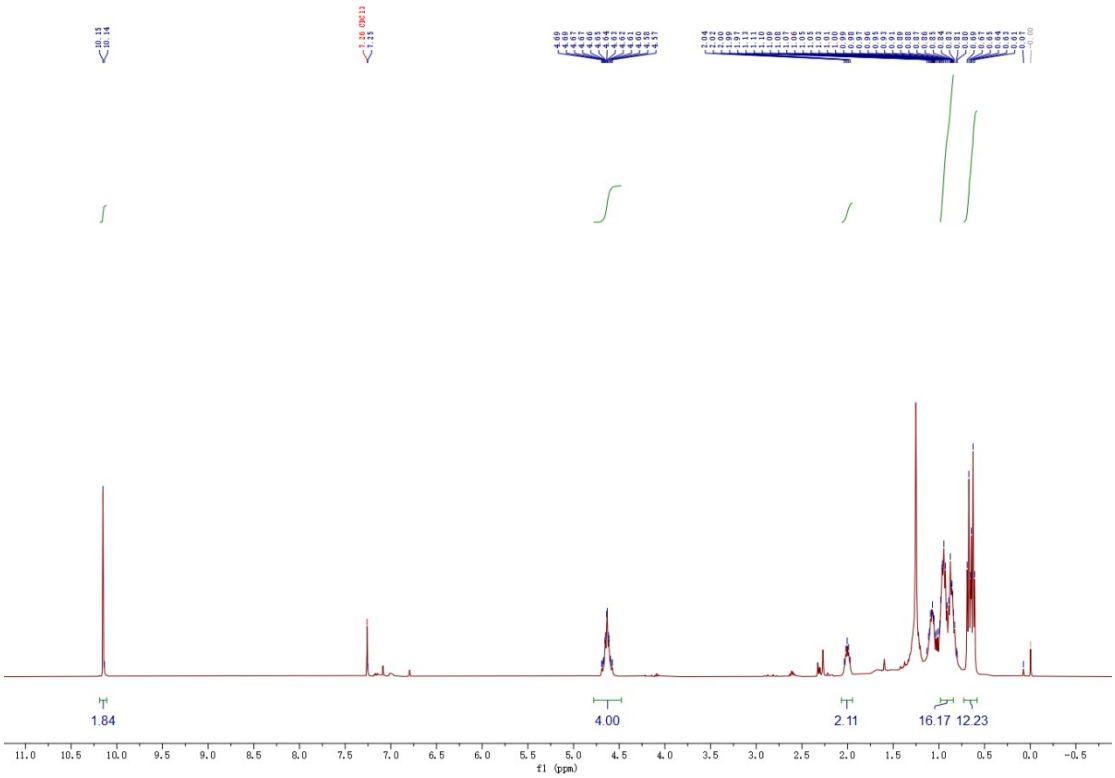

Figure S12. ^{1}H NMR (400 MHz) of **compound 3**.

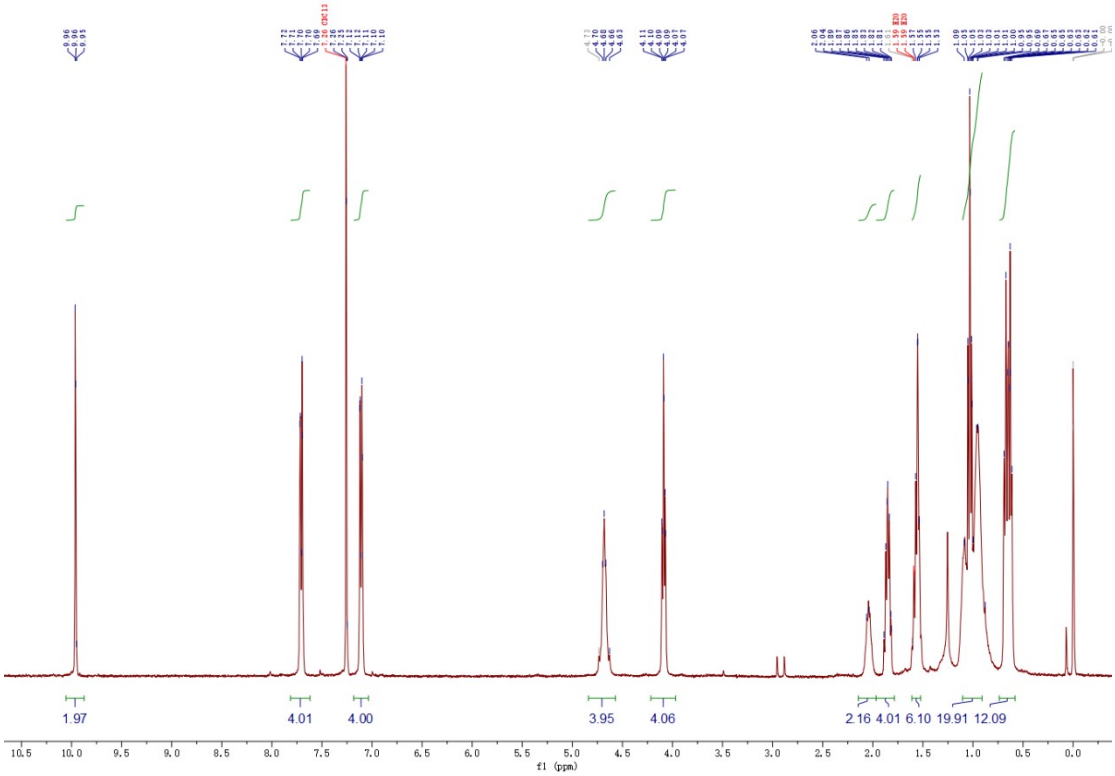

Figure S13. ^{1}H NMR (400 MHz) of compound **BTP-OC4-CHO**.

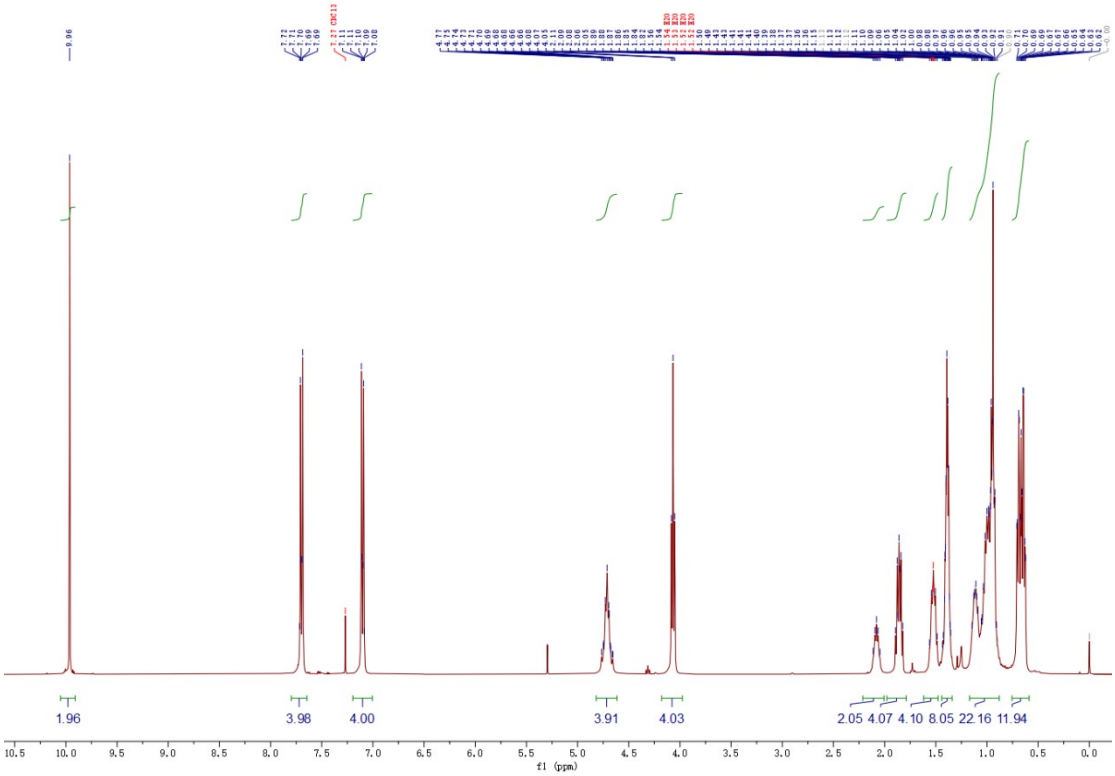

Figure S14. ^{1}H NMR (400 MHz) of compound **BTP-OC6-CHO**.

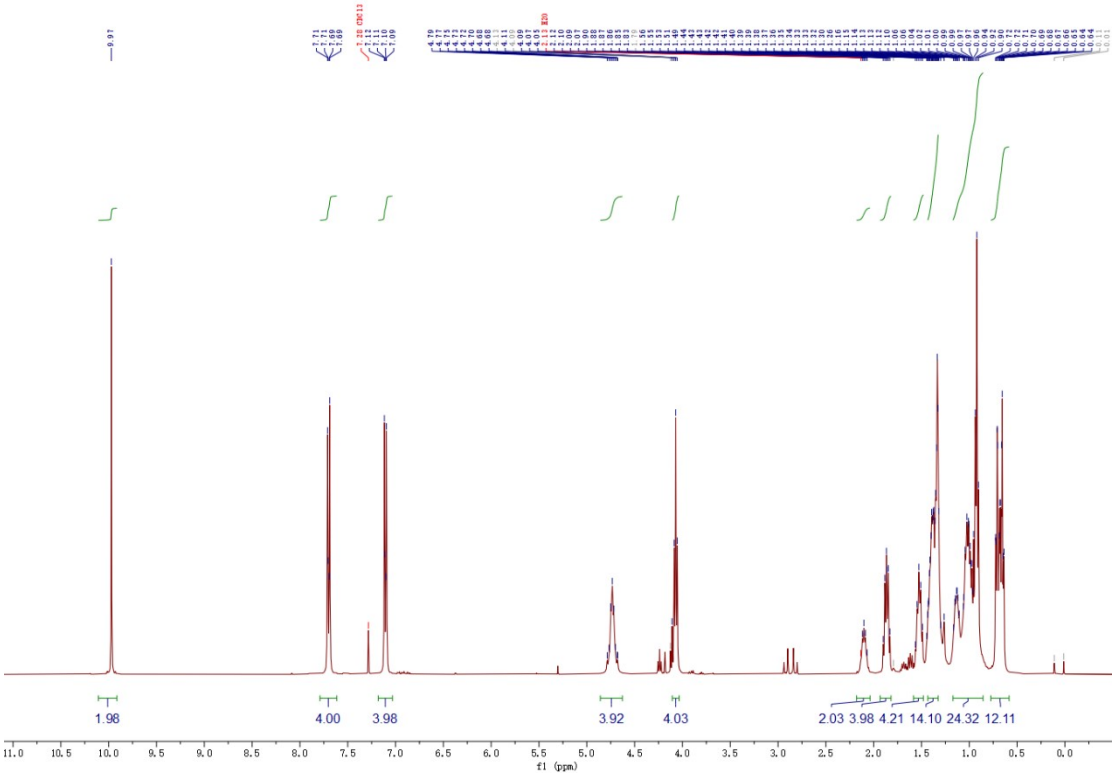

Figure S15. ^{1}H NMR (400 MHz) of compound **BTP-OC8-CHO**.

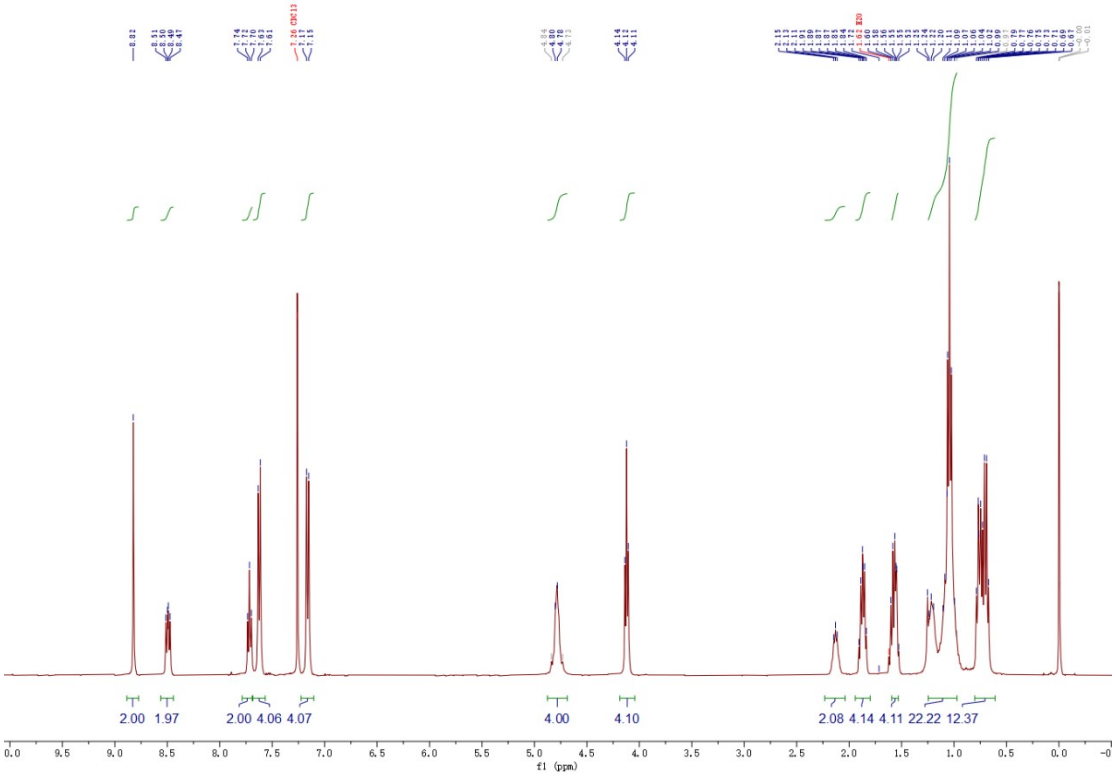

Figure S16. ^{1}H NMR (400 MHz) of compound **BTP-OC4**.

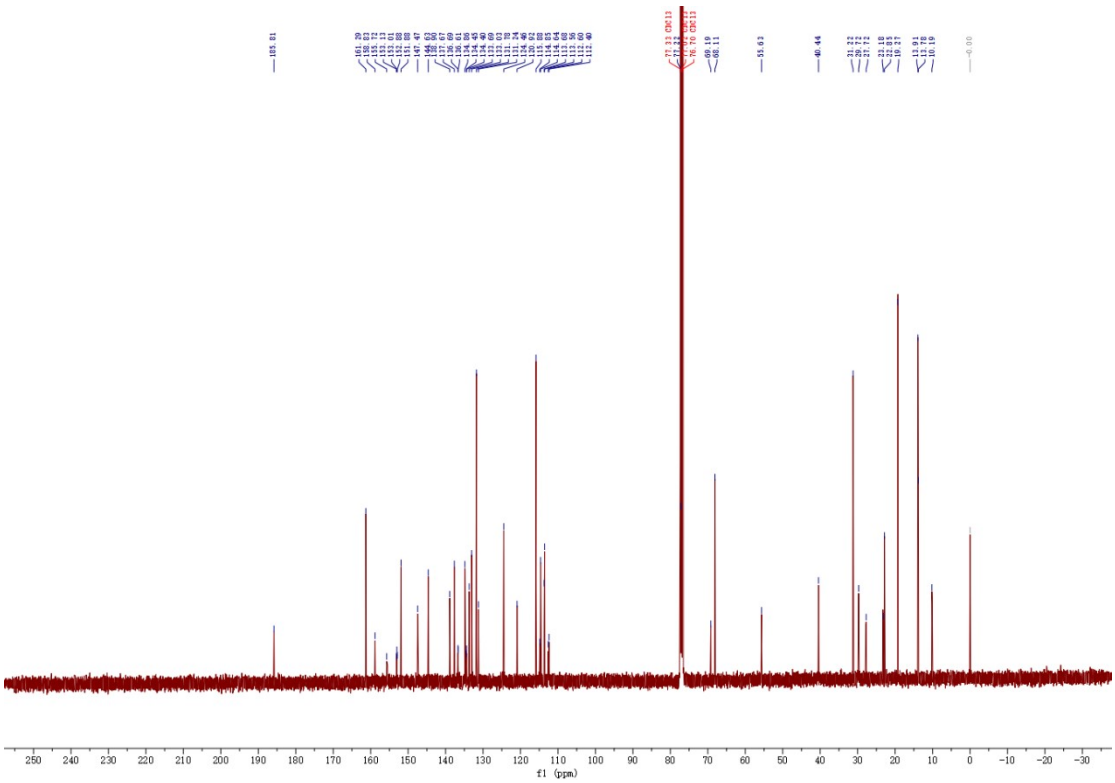

Figure S17. ^{13}C NMR (101 MHz) of compound **BTP-OC4**.

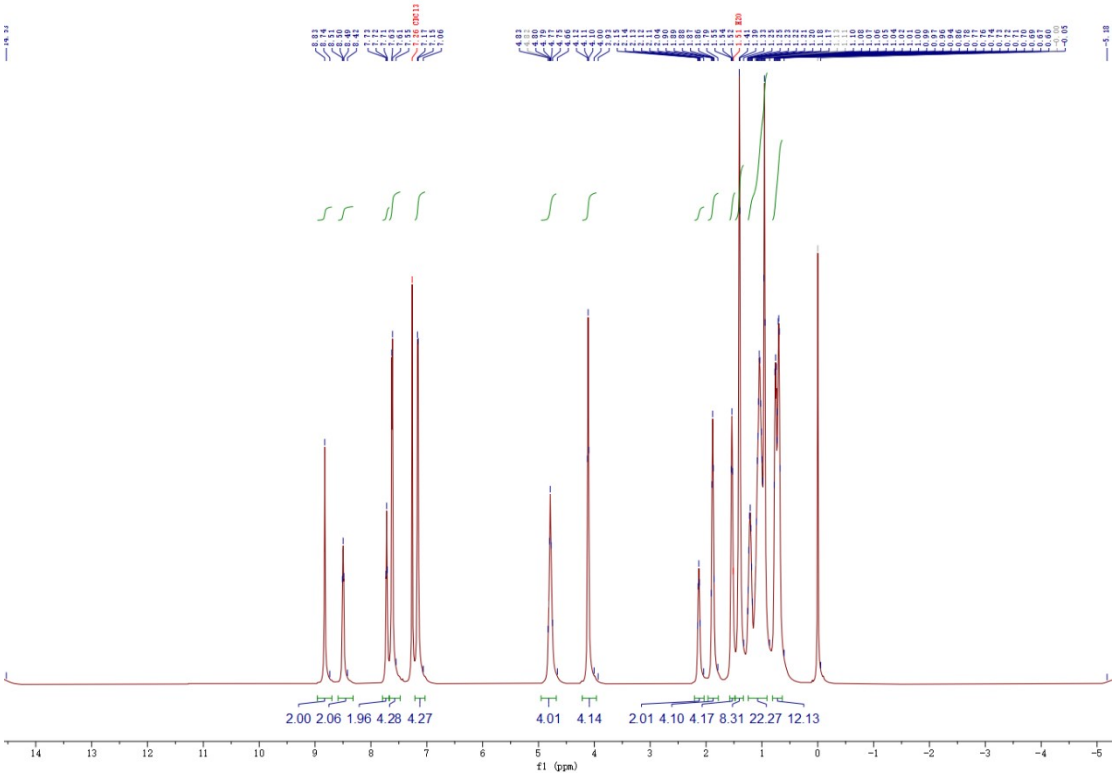

Figure S18. ^{1}H NMR (600 MHz) of compound **BTP-OC6**.

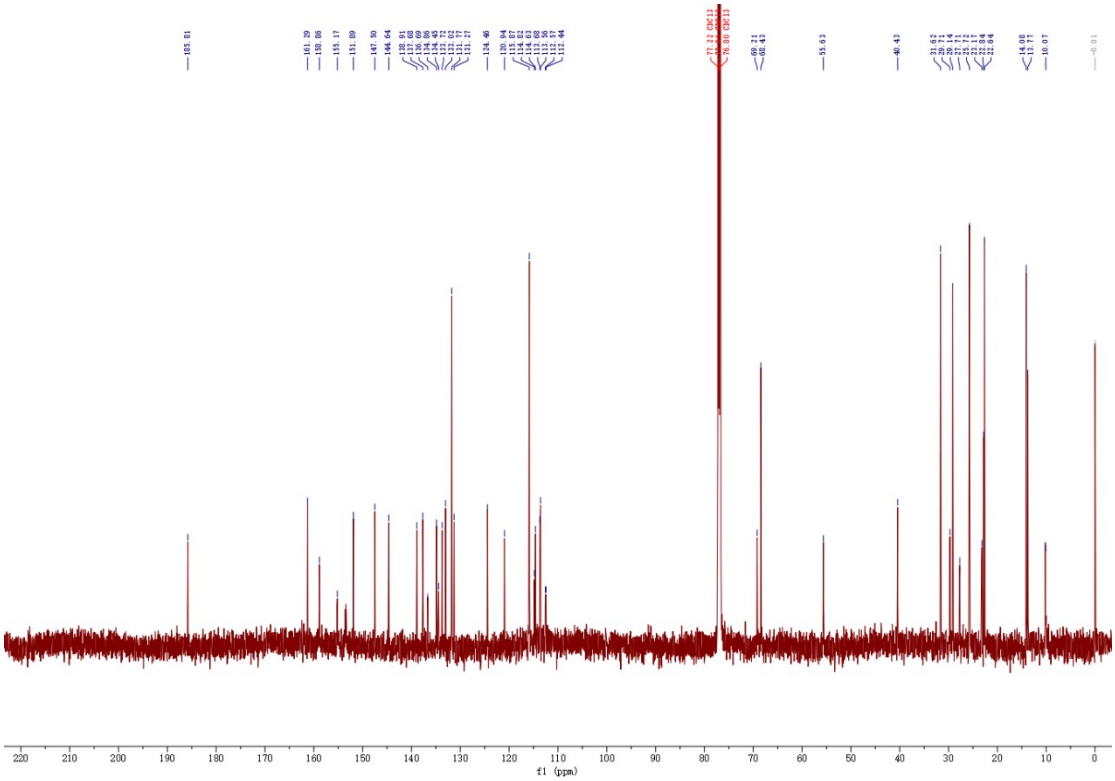

Figure S19. ^{13}C NMR (151 MHz) of compound **BTP-OC6**.

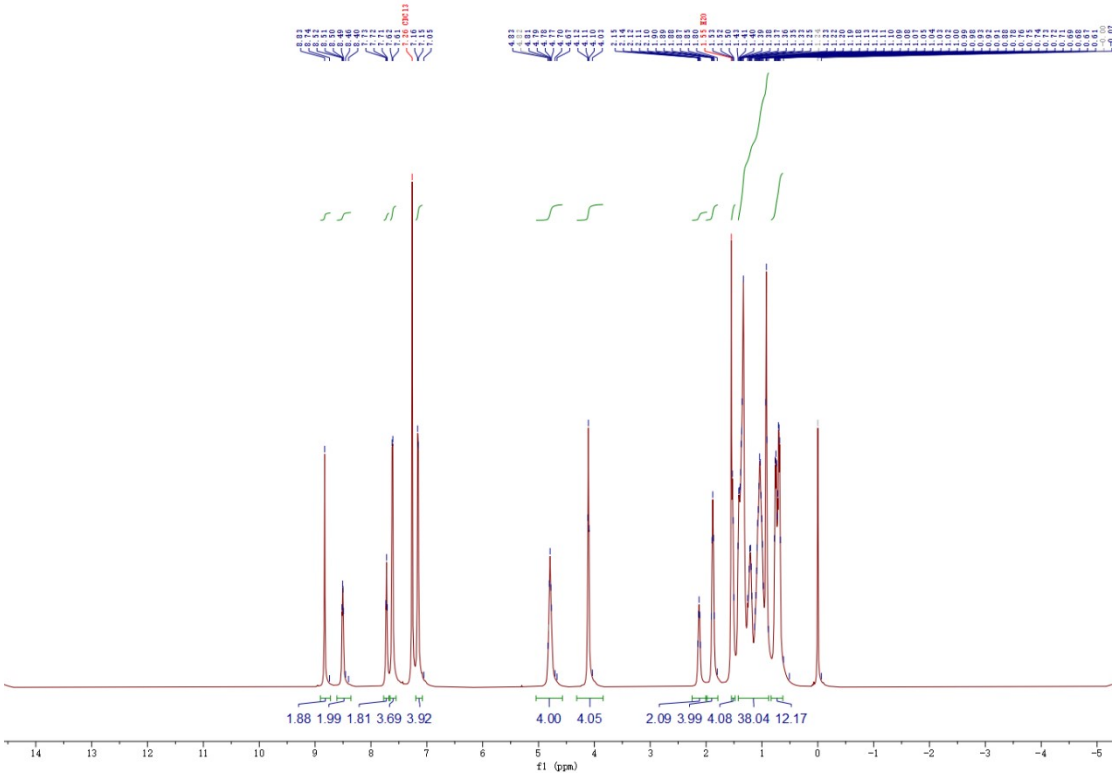

Figure S20. ^{1}H NMR (600 MHz) of compound **BTP-OC8**.

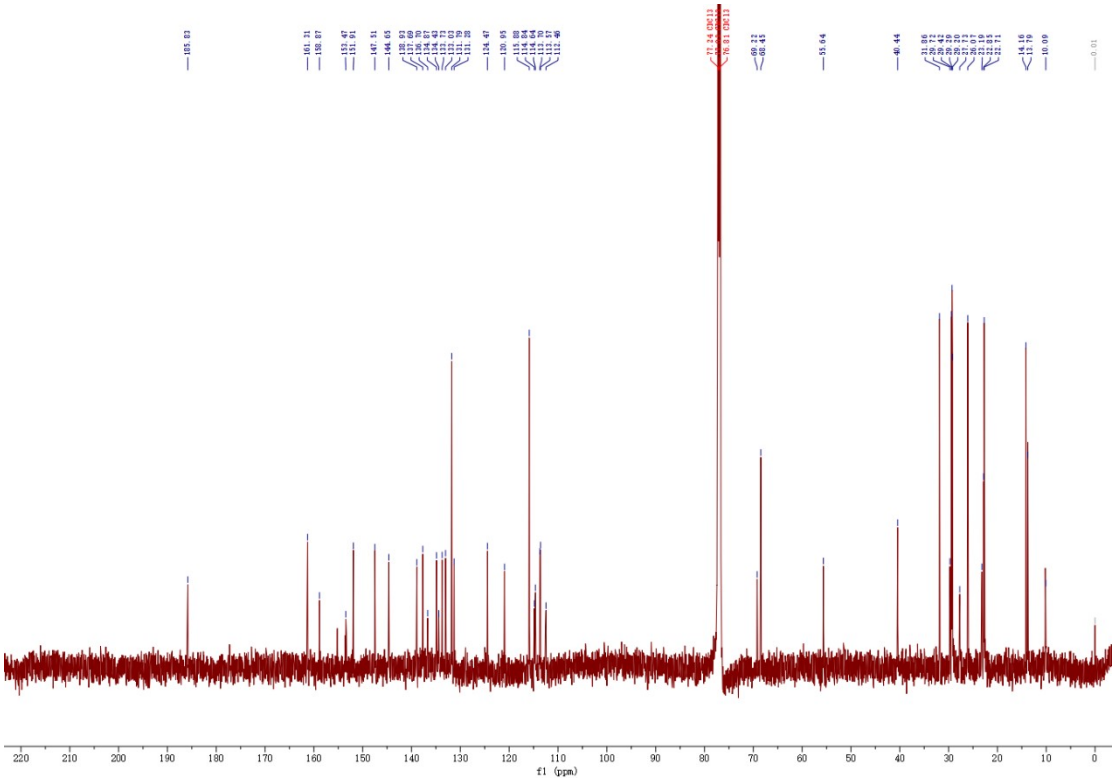

Figure S21. ^{13}C NMR (151 MHz) of compound **BTP-OC8**.

7. References

1. J. Zhang, F. Bai, I. Angunawela, X. Xu, S. Luo, C. Li, G. Chai, H. Yu, Y. Chen, H. Hu, Z. Ma, H. Ade and H. Yan, *Adv. Energy. Mater.*, 2021, **11**, 2102596.
2. K. Jiang, Q. Wei, J. Y. L. Lai, Z. Peng, H. K. Kim, J. Yuan, L. Ye, H. Ade, Y. Zou and H. Yan, *Joule*, 2019, **3**, 3020-3033.
3. G. Chai, Y. Chang, J. Zhang, X. Xu, L. Yu, X. Zou, X. Li, Y. Chen, S. Luo, B. Liu, F. Bai, Z. Luo, H. Yu, J. Liang, T. Liu, K. S. Wong, H. Zhou, Q. Peng and H. Yan, *Energy Environ. Sci.*, 2021, **14**, 3469-3479.
4. X. Kong, C. Zhu, J. Zhang, L. Meng, S. Qin, J. Zhang, J. Li, Z. Wei and Y. Li, *Energy Environ. Sci.*, 2022, **15**, 2011-2020.
5. G. Chai, Y. Chang, Z. Peng, Y. Jia, X. Zou, D. Yu, H. Yu, Y. Chen, P. C. Y. Chow, K. S. Wong, J. Zhang, H. Ade, L. Yang and C. Zhan, *Nano Energy*, 2020, **76**, 105087.
6. Y. Cui, H. Yao, J. Zhang, K. Xian, T. Zhang, L. Hong, Y. Wang, Y. Xu, K. Ma, C. An, C. He, Z. Wei, F. Gao and J. Hou, *Adv. Mater.*, 2020, **32**, e1908205.
7. Y. Chen, T. Liu, L.-K. Ma, W. Xue, R. Ma, J. Zhang, C. Ma, H. K. Kim, H. Yu, F. Bai, K. S. Wong, W. Ma, H. Yan and Y. Zou, *J. Mater. Chem. A.*, 2021, **9**, 7481-7490.
8. S. Chen, L. Feng, T. Jia, J. Jing, Z. Hu, K. Zhang and F. Huang, *Sci. China Chem.*, 2021, **64**, 1192-1199.
9. C. Li, J. Zhou, J. Song, J. Xu, H. Zhang, X. Zhang, J. Guo, L. Zhu, D. Wei, G. Han, J. Min, Y. Zhang, Z. Xie, Y. Yi, H. Yan, F. Gao, F. Liu and Y. Sun, *Nat. Energy*, 2021, **6**, 605-613.